Tunnelling and Underground Space Technology 157 (2025) 106314

Contents lists available at ScienceDirect

Tunnelling and Underground Space Technology incorporating Trenchless Technology Research

journal homepage: www.elsevier.com/locate/tust

Estimation of settlement-induced damage in masonry buildings from displacement measurements

Yiyan Liu [a,*], Harvey Burd [a], Derya Burcu Gulen [a], Korhan Deniz Dalgic [b], Ben Gilson [c], Alper Ilki [d], Sinan Acikgoz [a]

[a] Department of Engineering Science, University of Oxford, 15 Parks Road, Oxford, OX1 3PJ, UK
[b] Civil Engineering Department, Izmir Institute of Technology, Gulbahce Campus, Urla, Izmir 35430, Turkey
[c] Infrastructure Geotechnics Division, Arup, 8-13 Fitzroy Street, London W1T 4BQ, UK
[d] Department of Civil Engineering, Istanbul Technical University, Maslak 34469, Istanbul, Turkey

ARTICLE INFO

Keywords:
Large-scale testing
Deformation measures
Masonry
Tensile strain – damage correlation
Settlement
Excavation

ABSTRACT

In current engineering practice, building damage due to nearby ground excavation activities is typically quantified by processing displacement measurements. Building displacements at discrete points are used to determine deflection measures (such as angular distortion) which are then employed to estimate building strains using elastic beam models; damage is subsequently categorised according to the limiting tensile strain criteria. The reliability of this procedure relies on the extent to which the equivalent beam models employed in the analysis provide a realistic representation of the building behaviour. However, few published investigations are available on this issue. The current paper provides an appraisal of displacement-based building damage estimation techniques by employing digital image correlation displacement data collected from a recent experimental campaign on the settlement response of three half-scale masonry buildings. The results demonstrate that the treatment of buildings with equivalent beam models does not capture building deformation kinematics, potentially leading to inaccurate estimations of damage severity and location. An alternative strain interpretation procedure, inspired by an equivalent frame idealisation of a building façade with openings, is proposed. This procedure, which uses a limited number of displacement measurements, offers a robust interpretation of strains. Its effectiveness in estimating damage is assessed through experimental data. It is demonstrated that the current limiting tensile strain criteria need to be modified to provide a reliable estimation of crack widths when using the equivalent frame idealisation.

1. Introduction

Tunnelling and deep excavation in soft ground inevitably leads to ground movements (Mair, 1998); these movements can cause damage to existing buildings (ITA/AITES, 2011). Masonry buildings are especially vulnerable to ground movement-induced cracking damage due to their relatively low tensile strength (Boscardin and Cording, 1989; Burland and Wroth, 1974).

Urban projects involving underground construction typically require the monitoring of at-risk masonry buildings to evaluate the level of damage in the building and to support potential mitigation activities. The direct monitoring of the width of emerging cracks in masonry buildings is infeasible in most cases. Instead, monitoring operations typically involve the measurement of displacement at discrete points on the building (e.g. the measurement of horizontal and vertical displacements using prisms and precise levels in recent tunnelling projects (Crossrail Limited, 2008; High Speed Two Limited, 2017; Thames Water Utilities Limited, 2014). These displacement data are processed using an engineering model to estimate the distribution of tensile strain in the building. Then, by using empirical correlations between estimated maximum tensile strain and notional damage categories, building damage is classified.

In current practice, the internal strain distribution in a building is typically estimated by idealising the building as an elastic equivalent beam. A simplified modelling approach employing Timoshenko beam theory (Burland and Wroth, 1974) is commonly employed. This approach does not consider the influence of important building characteristics, such as façade openings (e.g. for windows and doors) and

* Corresponding author.
E-mail address: dimo.liu@gmail.com (Y. Liu).

https://doi.org/10.1016/j.tust.2024.106314
Received 13 March 2024; Received in revised form 20 November 2024; Accepted 4 December 2024
Available online 18 December 2024

floor structures (e.g. slabs). To account for these aspects, alternative equivalent beam formulations (e.g. Son and Cording, 2005; Finno et al., 2005) have been proposed.

Experimental evaluations of the robustness of current damage estimation approaches are limited. Giardina et al. (2013) used a 1/10 scale masonry model to appraise the performance of the Burland and Wroth (1974) approach; however, this study was limited to one specific type of building structure. Ritter et al. (2020) analysed the angular distortion and damage in six 3D-printed building specimens with varying building openings and tunnel eccentricity in a geotechnical centrifuge. The small length scale of these tests – 1/10 in the study by Giardina et al. (2013) and 1/75 in the study by Ritter et al. (2020) – makes it challenging to evaluate currently-used damage estimation techniques which relate crack width observations to tensile strain estimates.

In a recent test campaign, three half-size masonry building models were subjected to simulated tunnel-induced ground movements to explore the influence of ground movements on the development of visible cracking. The tests were conducted at the Fibrobeton factory site in Duzce, Turkey, between December 2020 and March 2021. Details on the prototype dimensions of the building being modelled, the design of the tests, the loadings that were applied and observations on the damage induced in the buildings are given in Dalgic et al. (2023). The tests incorporated a digital image correlation (DIC) system to measure the displacements at discrete targets on the masonry façade, with the setup and validation of the DIC monitoring system also described in detail in Dalgic et al. (2023). The current paper is concerned with the evaluation of procedures to use these displacement data to estimate the internal state of strain in the façade. In a preliminary investigation of data from one of the test buildings, Liu et al. (2022b) conducted a damage assessment using the Burland and Wroth (1974) equivalent beam formulation. The locations of the observed cracks were different from those that were predicted by beam theory; this indicates that the kinematic assumptions inherent in the beam model are a poor representation of reality in this case.

The current paper extends the earlier analysis by Liu et al. (2022b) by considering tests on two additional building models from the same testing campaign. Dalgic et al. (2023) indicated that the presence of additional façade openings and different floor structures in the two additional building models significantly influenced the initiation and propagation of observed damage. The ability of various beam idealisations to estimate strains in the building models and to categorise damage is first considered.

A separate ‘equivalent frame idealisation’ (EFI) approach is also explored; this approach forms the key innovation presented in the paper. The EFI approach employs separate beam kinematic models for each pier and spandrel in the masonry façade. This provides a means of estimating a strain field for the whole façade – based on a set of discrete displacement measurements – in a manner that respects the presence of openings for windows and doors. The equivalent frame idealisation is inspired by procedures – known as ‘equivalent frame models’ – which are used as the basis of computationally-efficient numerical models of masonry structures (e.g. Gulen et al. 2021, Lagomarsino et al. 2013); in equivalent frame models the piers and spandrels are represented as individual beams. It is emphasised, however, that EFI is solely a kinematic model for the purpose of estimating a strain field from discrete displacement measurements; the model makes no assumptions on the constitutive behaviour of the masonry.

Conclusions on the effectiveness of the EFI approach to quantify the state of damage in a masonry façade are primarily based on the analysis of two building models, with additional insights provided by two other cases, that were investigated in the testing campaign described in Dalgic et al. (2023). The current paper first summarises the test campaign (Section 2). This is followed by the formulation, demonstration and assessment of equivalent beam methods (Section 3) and the equivalent frame idealisation (Section 4) in the context of damage monitoring.

2. Large-scale building settlement test campaign

The tests comprise four L: 5.6 m $\times$ W: 3.2 m half-scale building models, as shown in Fig. 1a, with different window openings, weight arrangements and floor types. Each building model consists of two parallel façades constructed using brickwork and connected at first and second floor levels by either rigid reinforced concrete slabs or flexible joists simply supported on the façades. 7.8 tonnes of kentledge was placed at first and second floor levels of the building models (referred to as W1 weight) to simulate the in-situ stress level of prototype buildings at the model scale; the influence of additional kentledge loading was also investigated. A code is assigned to each test according to the number of window openings per storey (e.g. 50O stands for 5 and 0 openings on parallel façades), floor type (i.e. RF refers to rigid slab floor and JF refers to joist floor) and weight code (e.g. W3 refers to a load case with additional window sill loads weighing 3.3 tonnes to simulate suspended ground floor loading.). The building models are specified in Table 1.

To conduct a test, downward displacements (referred to as beam tip settlement , V_{tip}, see Fig. 1b) were applied to the beams supporting the building models by simultaneously pulling down the manual screw jacks at the free end of both beams (see Fig. 1a). This caused the beams to deform in a way that mimics the hogging region of a tunnel-induced settlement trough. One façade of each building model was installed with measurement targets (as shown in Fig. 1b). The displacements of these targets were continuously tracked using 2D DIC. At the end of each test (i.e. when the building is subjected to the maximum displacement applied in the test) the façade was inspected for damage. During this inspection, the precise location of visible cracks was recorded and their width was measured using a crack ruler. The crack locations and widths were also retrieved retrospectively from DIC data by calculating the relative displacement between targets orthogonal to the crack (see Liu et al., 2022b). The crack ruler and DIC measurements indicate consistent results. For brevity, only DIC crack measurements will be used in this paper.

Damage induced in the building is characterised by the width of cracks that develop in the masonry as the test progressed. Consistent with current industry practice, damage is quantified in terms of a ‘damage category’ that relates to the width of the widest crack that developed in the building. The Burland et al. (1977) correlation between crack width and damage category (indicated in the leftmost three columns of the Table A1 in Appendix A) is employed; this is referred to in this paper as ‘standard damage correlation’. ‘Negligible’ and ‘very slight’ damage categories are not differentiated in the current work (i.e. damage less severe than the ‘slight’ category is labelled as ‘negligible’); differentiation between these two categories is of limited practical importance and would require more accurate crack measurement systems than those used in the current work. Due to the one-half geometric scale adopted in the tests, the adopted crack widths relevant to the various damage categories are half of the prototype values (as recorded in the fourth column in Table A1). Table 2 records the beam tip settlement when each building model first enters a specific damage category based on the maximum measured crack width. The maximum beam tip settlement applied in each test is also reported.

A description of the damage induced in each building model, including the influences of the openings and the structural characteristics of the floors, is given in Dalgic et al. (2023). Key observations are as follows. (i) Damage is strongly influenced by the number of openings; the 5-opening façade of 5O0-RF-W1 experienced significantly more intense and widespread damage (i.e. more cracks and larger crack width) than the façades of the equivalent 3-opening model, 3O-RF-W1. (ii) The presence of reinforced concrete slab floors in the RF models act to reduce the incidence of damage in the first storey of the building; while the building with joist floors 3O-JF-W1 suffered brittle damage initiating from the first storey, the corresponding building with reinforced concrete slab floors 3O-RF-W1 did not. (iii) The 3O-RF-W1

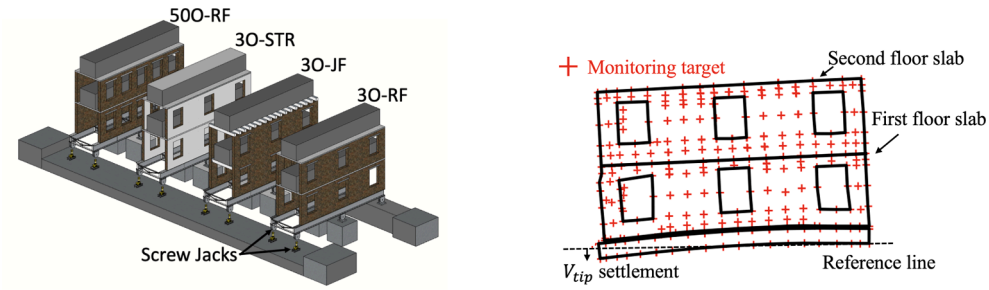

Fig. 1. (a) Building models and test setup (after Dalgic et al., 2023); (b) Schematic of 3O-RF building model with an induced beam tip settlement V_{tip}, red '+' indicates the monitoring target location, where displacement measurements are taken. (For interpretation of the references to colour in this figure legend, the reader is referred to the web version of this article.)

Table 1
Specification of the building models employed in the experimental campaign.

Building reference	Description
3O-RF	This building model comprises two similar masonry façades. At ground and first storeys of each façade, there are three openings (signified by the code 3O). Reinforced concrete slabs (signified by code RF) were cast at first and second floor levels. The building was initially loaded with weight configuration W1 (3O-RF-W1) and tested on 22 December 2020. Since this resulted in minimal observed damage the building was loaded with a different configuration of weights W3 and tested (3O-RF-W3) again on 28 January 2021.
3O-JF	This building model comprises two similar masonry façades with three openings (signified by the code 3O) at ground and first storeys. Reinforced concrete joists (signified by code JF to denote 'joist floor') were placed at first and second floor levels. A single test 3O-RF-W1 was conducted on this building on 11 February 2021.
3O-STR	This building model was employed in a separate research activity and is not considered further in the current paper.
50O-RF	This building model comprises two different masonry façades. One façade had five openings at ground and first storey levels and the other was plain masonry. Reinforced concrete slabs were cast at first and second floor levels. A single test 50O-RF-W1 was conducted on this building on 18 February 2021. Analysis of damage was confined to the façade containing the openings.

building deformed in an essentially rigid manner with minimal observed damage; gaps formed between the base of the building and the supporting beam. When 3O-RF-W1 was repeated with additional window sill loads (3O-RF-W3) the building conformed more closely to the applied beam displacements with a consequential increase in the severity of damage.

3. Estimation of building damage using equivalent beam idealisations

There are three steps to estimate building damage using displacement measurements and equivalent beam idealisations. First, displacement measurements are used to determine distortion measures, which describe various differential displacements and rotations experienced across the building. Second, distortion measures are used to estimate strains, using a beam idealisation. Finally, maximum tensile strains in the equivalent beam model are associated to a damage category, using established correlations. The application of these procedures to the test buildings is described below.

3.1. Distortion measures

Following current practice, the chosen distortion measures are 'deflection ratio', 'angular distortion' and 'average horizontal strain'. Deflection ratio Δ/L is defined as indicated in Fig. 2a where Δ is maximum vertical displacement with respect to a straight reference line between the corners of the building, with length L. The angular distortion β is equivalent to the overall shear deformation of a particular bay of the building (Fig. 2b):

$$\beta_{\mathrm{ABCD}} = -\left[\frac{(V_B + V_C) - (V_A + V_D)}{2L_{BAY}}\right] + \frac{(U_D + U_C) - (U_A + U_B)}{2H} \tag{1}$$

where U_p, V_p are the horizontal and vertical displacement at a general point P and β_{ABCD} is the angular distortion for a building bay defined by the points A, B, C and D (see Fig. 2b). The building bay length and height are denoted by L_{BAY} and H.

Additionally, values of 'average horizontal strain' are employed in conjunction with deflection ratio and angular distortion. For the building bay in Fig. 2b, average horizontal strain ε^h_{AB} is calculated as:

$$\varepsilon^h_{AB} = \frac{U_B - U_A}{L_{BAY}} \tag{2}$$

3.2. Strain estimation

3.2.1. Deep beam approach (DBA)

In the widely-used approach by Burland and Wroth (1974) the building is represented by a homogeneous elastic Timoshenko beam with a uniform rectangular cross-section. The presence of openings and floors is neglected. In the current paper, this approach is referred to as the 'Deep Beam Approach' (DBA).

Table 2
Summary of damage categories based on the measured maximum crack width, w. Values recorded under each damage category are the beam tip settlement at which the building model first enters that damage category. The final damage category is the damage category of the building model when the maximum beam tip settlement is reached.

Test code	Max beam tip settlement (mm)	Slight (mm) ($0.5 < w < 2.5$) mm	Moderate (mm) ($2.5 < w < 7.5$) mm	Severe (mm) ($7.5 < w < 12.5$) mm	Very severe (mm) ($w > 12.5$) mm	Final damage category (at maximum tip settlement)
3O-RF-W1	67	7.8	–	–	–	Slight
3O-RF-W3	35	9.6	16.7	33.2	–	Severe
50O-RF-W1	26	7.3	15.7	–	–	Moderate
3O-JF-W1	32	9.4	31.9	31.9	31.9	Very severe

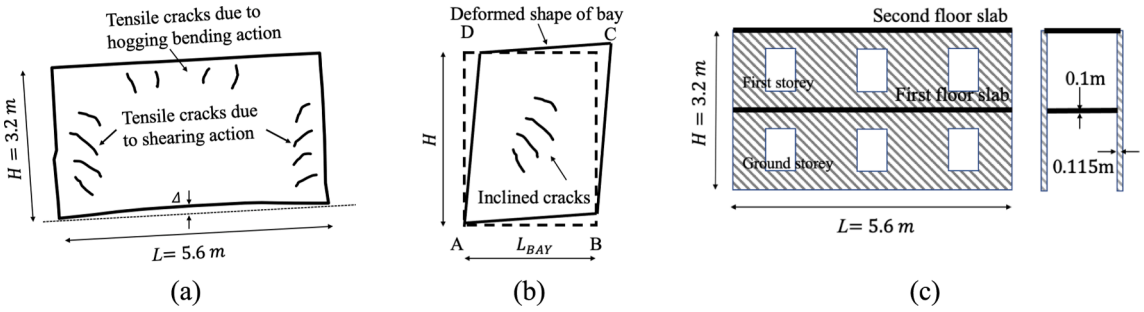

Fig. 2. (a) Assumed deformation mode and potential crack locations for Deep Beam idealisation of a building façade with a neutral axis at the base. The location of diagonal cracks is not prescribed in Burland and Wroth (1974) but are expected to concentrate around the neutral axis; (b) Bay Beam idealisation of a building bay with an imposed angular distortion. The inclination of the cracks will depend on the ratio between angular distortion, β, and average horizontal strain ε^h_{AB} at the base of the bay; (c) Sandwich Beam idealisation of a building façade and dimensions of a cross-section of the building models.

To apply the DBA to a building deforming in hogging (as in the current tests) it is considered that the neutral axis lies at the base of the building. In this case the maximum tensile strain due to bending, ε^t_b, is related to the deflection ratio Δ/L (determined from the measured displacements of the lowest level of DIC markers fixed to the facade) by,

$$\frac{\Delta}{L} = \left\{\frac{L}{12H} + \frac{EH}{2LG}\right\}\varepsilon^t_b \tag{3}$$

where E and G are Young's and shear moduli of the equivalent beam. The ratio E/G is taken as 2.6 in this paper following Mair et al. (1996). Separately, the maximum tensile strain due to shear, ε^t_s, is,

$$\frac{\Delta}{L} = \left\{1 + \frac{GL^2}{6H^2E}\right\}\varepsilon^t_s \tag{4}$$

Additionally, the average horizontal strain ε^h developed at the base of the building (determined from horizontal displacement measurements) is combined with ε^t_b and ε^t_s (using a tensor-based approach, e.g. Boscardin and Cording, 1989) to determine the maximum tensile strain ε^t_{max} experienced by the building. According to this model, if the maximum tensile strain is due to bending and its magnitude exceeds a limiting value, visible vertical cracks would be expected at the top of the building at its midspan location (see Fig. 2a). Conversely if shear effects are dominant then visible inclined cracks would be expected to occur towards the edges of the façade (Fig. 2a).

3.2.1.1. Sandwich beam approach (SBA). Finno et al. (2005) proposed an alternative equivalent beam model referred to as the Sandwich Beam Approach (SBA). This approach is relevant for buildings with stiff floor slabs. In SBA, bending resistance is provided by the floors; the masonry walls act only in shear (see Fig. 2c). SBA incorporates an explicit consideration of floor stiffness and the geometry of openings in the façade.

The SBA approach is only applicable to the two rigid floor building models (3O-RF and 50O-RF). To apply SBA to these models, two slabs (first floor slab and second floor slab) and two load-bearing walls (ground storey and first storey) are considered, as shown in Fig. 2c. When determining the shear stiffness of the wall, the influence of window openings is considered via a reduced wall shear area $A_{v,\,wall}$. Consistent with DBA, the neutral axis of the sandwich beam is assumed to coincide with the base of the façade. The maximum tensile strain due to bending, ε^t_b, is determined as,

$$\frac{\Delta}{L} = \left[\frac{L}{12H} + \frac{E_{slab}I_{slab}}{G_{wall}\overline{A_{v,wall}}LH}\right]\varepsilon^t_b \tag{5}$$

where $E_{slab}I_{slab}$ is the bending stiffness of the equivalent sandwich beam, determined by the slab properties, floor area, and the location of the slabs relative to the neutral axis, while $G_{wall}\overline{A_{v,wall}}$ is the shear stiffness of the equivalent sandwich beam, determined by the shear area and shear modulus of the infill walls. The maximum tensile strain due to shear, ε^t_s, is found by,

$$\frac{\Delta}{L} = \left[\frac{L^2(G_{wall}\overline{A_{v,wall}})}{18E_{slab}I_{slab}} + 1\right]\varepsilon^t_s \tag{6}$$

Similar to DBA, ε^t_b and ε^t_s are combined with the horizontal strain, ε^h; the largest value of the resulting tensile strain is considered to be ε^t_{max}.

In the current work, Young's modulus E_{slab} of the reinforced concrete slab and shear modulus G_{wall} of the infill wall are based on the values employed in the numerical analyses conducted by Dalgic et al. (2021). The second moment of area of the slab I_{slab} and total shear area $\overline{A_{v,wall}}$ are derived based on the dimension of each building model. The relevant data are summarised in Table 3.

3.2.1.2. Bay beam approach (BBA). In an alternative mechanical representation (referred to as Bay Beam Approach, BBA, Son and Cording, 2005) the building is considered as a series of shear deformable rectangular 'bays' (see Fig. 2b). The deformation of each bay is defined by the value of angular distortion determined from the monitored displacements. The shear strain is assumed to be uniform within each bay; it is therefore equal to angular distortion (Equation (1). The shear strain is combined with average horizontal strain (averaged over the length of the bay) using a tensor-based approach to determine a value of ε^t_{max} relevant to the façade. Since bending effects are neglected and constant shear and axial deformation is assumed, there is no particular expected location for the emergence of visible cracks. The definition of bays is somewhat arbitrary, although previous studies define them around façade openings (Cook, 1994; Ritter et al., 2020). This approach in which bays are defined around façade openings – as adopted in the current paper – provides for a consistent segmentation of the façade for strain analysis.

3.3. Tensile strain and damage category correlation

The value of maximum tensile strain ε^t_{max} determined from equivalent beam models is correlated to a damage category. In the current

Table 3
Material properties, second moment of area and total shear area used in SBA for 50O-RF-W1 and 3O-RF-W1/W3.

	E_{slab}(GPa)	G_{wall}(GPa)	I_{slab}(m^4)	$\overline{A_{v,wall}}$(m^2)
50O-RF-W1 (35 % window opening ratio)	32	1.435	0.844	0.112
3O-RF-W1/W3 (20 % window opening ratio)	32	1.435	0.844	0.138

paper, the standard damage correlation in Table A1 is used (employing equivalent crack width for half-scale tests). It should be noted that while the crack widths are scaled by the geometric factor employed in the building models, the limiting tensile strain values presented in the table are not scaled due to their dimensionless nature. This correlation was formulated in an empirical manner, employing data and observations from various laboratory tests and field cases (e.g. Skempton and MacDonald, 1956) combined with tensile strain estimates from equivalent beam models.

4. Performance evaluation of equivalent beam models

4.1. Three-opening building models

4.1.1. 3O-RF tests

The first building model to be tested in the campaign was 3O-RF. Initially this was loaded with configuration W1 and then tested to an applied beam tip settlement of 67 mm. The building suffered minimal observable damage, with a single visible crack in a ground storey spandrel (see Fig. 3c). Data on maximum tensile strain determined using the beam models (DBA and SBA) are shown in Fig. 3a. To apply the BBA the building was considered in three separate bays. Calculated values of ε^t_{max} for each of the bays are shown in Fig. 3b. All three modelling approaches indicate that the damage category is 'negligible'. The dominant damage mode of DBA and SBA is bending and shearing, respectively. Their implied damage patterns are shown in Fig. 3a inset.

Building deformed shape and crack observations are shown in Fig. 3c. In contrast to DBA, SBA and BBA predictions, the presence of a crack indicates the damage category as 'slight'. Contrasting Fig. 3c with Fig. 3a (inset), the location of this crack at one of the ground storey lower spandrels also contradicts DBA and SBA indications. The equivalent beam models are unable to provide an accurate indication of the intensity and location of the actual damage in this case. It appears that the cracked spandrel is subjected to a localised hogging displacement with the consequential formation of a vertical crack at its upper edge. Fig. 3d plots the evolution of horizontal displacements along the left vertical edge of the façade. The linear variation of horizontal displacements along the height indicates that the plane section at the edge of the building model remains plane, which is also evident in the deformed shape in Fig. 3c.

The slight damage experienced by 3O-RF-W1 provided an opportunity to re-test the building with additional window sill loads (W3) to induce additional damage to the building. Cracks that developed during test 3O-RF-W3 are shown in Fig. 4c. (Note that in this figure and in subsequent figures the order of the numerical labelling of the cracks is arbitrary). In this case significant cracking occurred at the ground storey of the façade; the first storey appeared undamaged. Horizontal cracks – which appeared to be induced by bending action – were observed at the

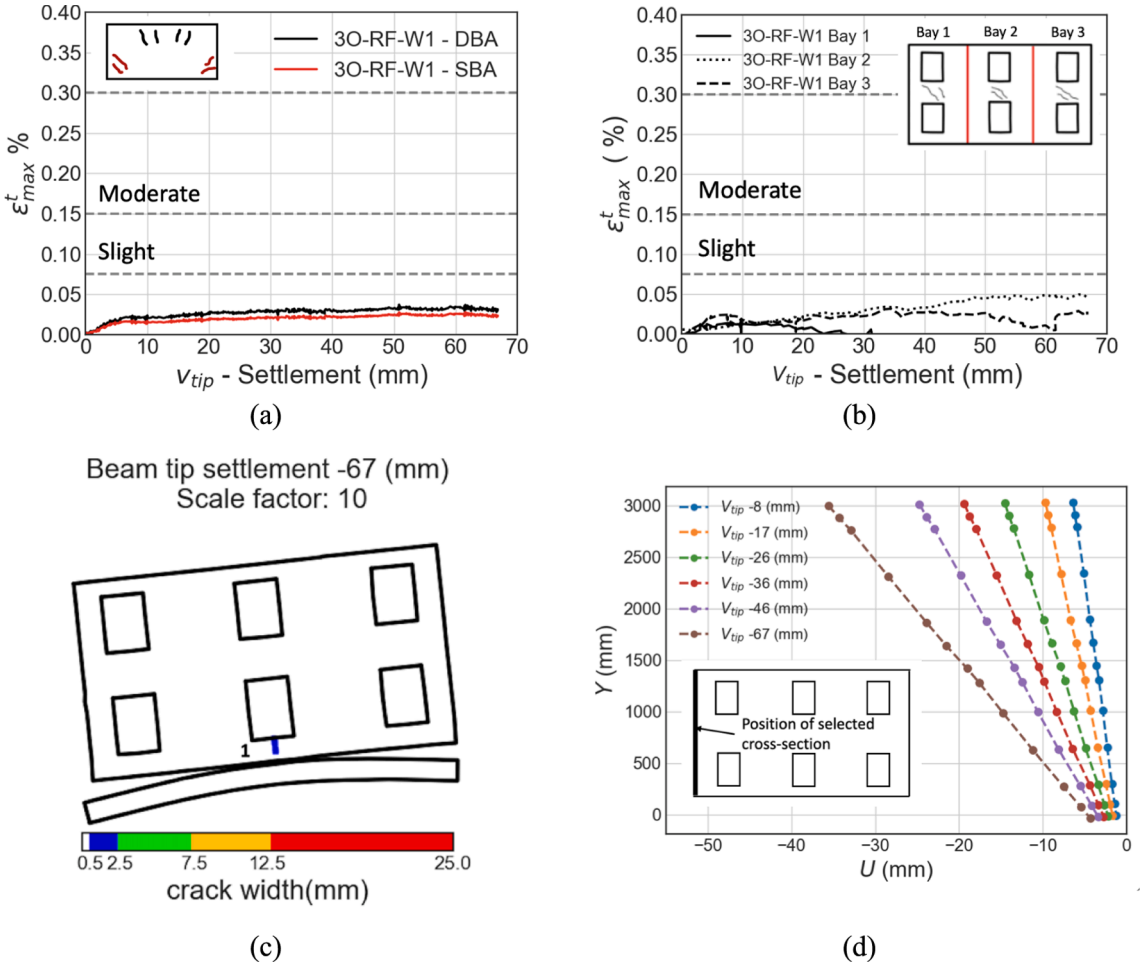

Fig. 3. (a) Values of maximum tensile strain ε^t_{max} estimated from measured values of deflection ratio and average horizontal strain for 3O-RF-W1 using the DBA (Black) and SBA (Red). Inset, the locations of cracks that would be predicted by the DBA (Black) and SBA (Red) are illustrated; (b) Values of maximum tensile strain ε^t_{max} determined from angular distortion and average horizontal strain using the BBA for 3O-RF-W1. The division of bays is shown in the inset; (c) Deformed shape of the front façade of 3O-RF-W1 at a beam tip settlement of 67 mm, plotted with the crack location and size (indicated by the colour bar where blue signifies 'slight' damage). (d) Profiles of the cross-section at the left edge of the building model for different beam tip settlements for 3O-RF-W1. (For interpretation of the references to colour in this figure legend, the reader is referred to the web version of this article.)

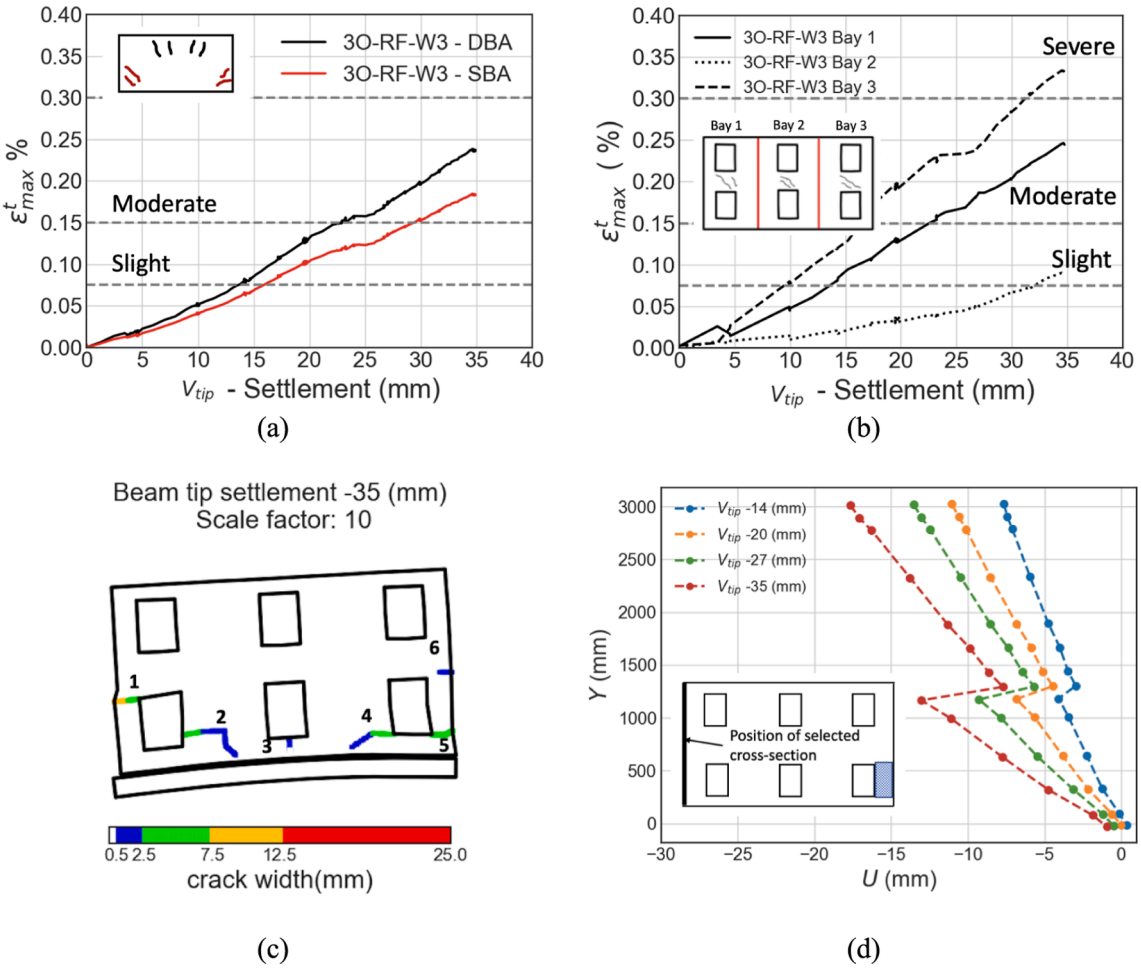

Fig. 4. (a) Values of maximum tensile strain ε^t_{max} estimated from measured values of deflection ratio and average horizontal strain on 3O-RF-W3 using the DBA (Black) and SBA (Red). Inset, the locations of cracks implied by DBA (Black) and SBA (Red) are illustrated. Horizontal dashed lines indicate boundaries between implied damage categories; (b) Values of maximum tensile strain ε^t_{max} determined from angular distortion and average horizontal strain using the BBA on 3O-RF-W3. The division of bays is shown in the inset; (c) Deformed shape of the front façade of 3O-RF-W3 at the beam tip settlement of 35 mm, plotted with the crack location and size (indicated by the colour bar where blue and green signify 'slight' and 'moderate' damage respectively); (d) Profiles of the cross-section at the left edge of the building model subjected various beam tip settlements in 3O-RF-W3. (For interpretation of the references to colour in this figure legend, the reader is referred to the web version of this article.)

slender external piers. Meanwhile, stockier internal piers experienced diagonal cracking. Based on the maximum width of the visible cracks, the building damage category was classified as 'severe' at the end of the test. Estimated values of ε^t_{max} from the beam models are shown in Fig. 4a-b. It is seen that the most onerous case from the BBA (Bay 3) indicates 'severe' damage at the end of the test, consistent with the observed damage state. The DBA and SBA approaches, however, classify the damage as 'moderate'. Location of cracks implied by DBA and SBA (shown inset in Fig. 4a) are not consistent with the damage observations in Fig. 4c. The horizontal deformation profiles along the left vertical edge of the building are shown in Fig. 4d. There appear to be two lines in this figure with distinct deformation trends, corresponding to the ground and first storey deformations. These lines indicate that building cross-sections do not remain plane due to crack formation at the top of external piers, violating kinematic assumptions in the formulation of DBA and BBA.

4.1.2. 3O-JF-W1 test

Fig. 5a shows data on beam tip settlement vs tensile strain determined using DBA for 3O-JF-W1 (since 3O-JF-W1 does not incorporate a rigid slab, SBA was not examined in this case). At beam tip settlements less than 32 mm, the estimated maximum tensile strains are similar to the data from the corresponding rigid floor test (3O-RF-W1, Fig. 3a). At the tip displacement of 32 mm the sudden development of significant cracks caused the building to deform and the gaps between the steel beam and the building to close (contrast the deformed shapes in Fig. 3c and 5c). The measured deflection ratio increased with a consequential increase in ε^t_{max}, as indicated in Fig. 5a. DBA estimates the final damage state as 'moderate'. The BBA approach (Fig. 5b) predicts a comparatively low level of strain and estimates 'slight' damage at the final state.

Deformed shape and crack widths at the maximum beam tip settlement in 3O-JF-W1 test are shown Fig. 5c. There was only slight damage in the building until two vertical cracks (cracks 1 and 2 in Fig. 5c) suddenly appeared at a tip settlement of 32 mm. These led to the development of cracks 3 and 4 at ground storey level. A maximum crack width of 40.45 mm was observed at the end of the loading for crack 2. This 'very severe' damage caused a partial collapse of the central lintel at the top. Actual damage severity was underestimated by the beam models. However, in this case, the location of damage at the first storey of the building at midspan location (shown inset Fig. 5c) was well-predicted by DBA. This agreement in damage location is due to the beam-like behaviour of 3O-JF-W1 highlighted in Fig. 5d, where building cross-sections remained plane. The beam-like behaviour of 3O-JF-W1 also explains the poor performance of BBA in interpreting damage category; the shear beam kinematics that underly BBA do not consider bending deformations, resulting in an underestimation of damage at the

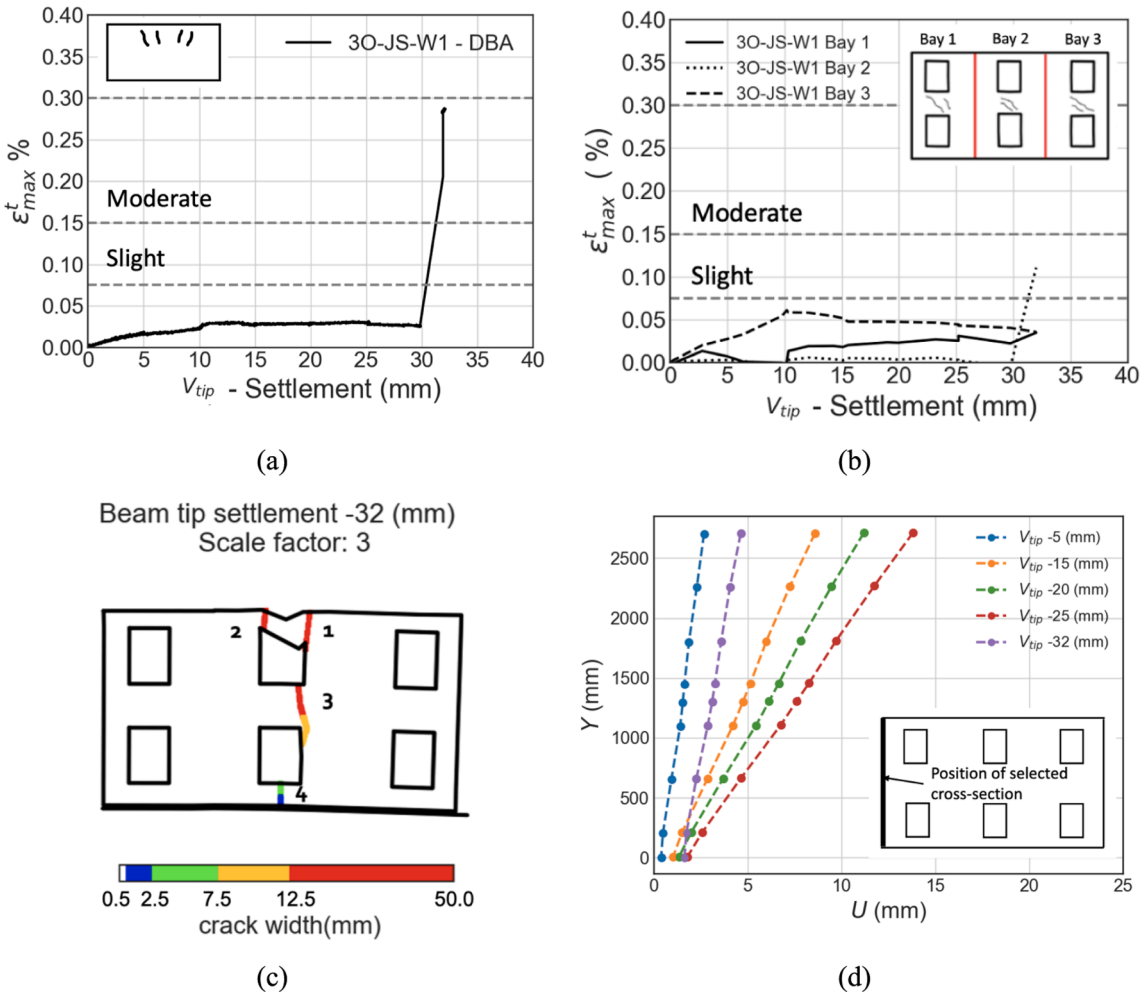

Fig. 5. (a) Values of maximum tensile strain ε^t_{max} estimated from measured values of deflection ratio and average horizontal strain for 3O-JF-W1 using the DBA. Inset, illustration of the crack locations implied by the tensile strains estimated by the DBA (Black); (b) Values of maximum tensile strain ε^t_{max} determined from angular distortion and average horizontal strain using the BBA for 3O-JF-W1; (c) Deformed shape of the front façade of 3O-JF-W1 at a beam tip settlement of 32 mm, plotted with the crack location and size (indicated by the colour bar where blue, green, orange and red signify 'slight', 'moderate', 'severe' and 'very severe' damage respectively). The deformed shape is displayed with an orientation that mirrors the perspective of facade-facing cameras; (d) Profiles of the cross-section at the left edge of the building model subjected various beam tip settlements for 3O-JF-W1. (For interpretation of the references to colour in this figure legend, the reader is referred to the web version of this article.)

final loading stage.

4.1.3. 50O-RF-W1 test

Fig. 6a shows the estimated maximum tensile strains from DBA due to bending, suggesting that at the end of the test (V_{tip} = 26mm) the building model has sustained moderate damage. The SBA indicates the building model was at the boundary between slight and moderate damage, with maximum strains due to shear. Fig. 6b shows that, at the end of the test, building bays 1, 2 and 4 are expected to experience moderate damage according to BBA, whereas – on the basis of the visible cracks – bays 3 and 5 experienced slight and moderate damage respectively. The beam models therefore all provide a consistent indication of moderate damage at the end of the test.

The observed crack damage in 50O-RF-W1 at the end of the test (see Fig. 6c) comprised horizontal cracks (cracks 1, 2, 6 and 7) at the ground storey external pier boundaries and vertical cracks (cracks 3, 4 and 5) on the ground storey spandrels. No diagonal cracks were observed; this is presumably due to the presence of windows causing individual slender building components to deform predominantly in bending. The horizontal crack (crack 1) at the top of the right external pier measured 6.02 mm at the final stage, corresponding to moderate damage category. Whilst the damage category indications from DBA and SBA are consistent with the intensity of the observed damage, crack locations (contrast Fig. 6c and Fig. 6a inset), the kinematics (contrast 'plane cross-section assumption' in beams with deformation profiles in Fig. 6d) disagree with observations.

4.2. Overall performance of the equivalent beam models

Table 4 summarises the performance of equivalent beam models in indicating damage category and location at the end of each test. The performance in indicating damage location is considered 'good' if the location of maximum tensile strain implied by the respective equivalent beam model corresponds to the actual cracking location; otherwise, it is considered 'poor'. The table highlights that the equivalent beam models tend to underestimate damage category and provide a poor indication of damage location.

Independent of the inconsistency of damage location and category predictions, the data presented in Section 4.1 appear to indicate a positive correlation between estimated strains and measured crack widths. The relationship between the maximum tensile strain determined from all equivalent beam models, plotted against actual maximum crack width determined from the DIC measurements is shown in Fig. 7. The data in Fig. 7a-b (relating to DBA and SBA) indicate an apparent linear

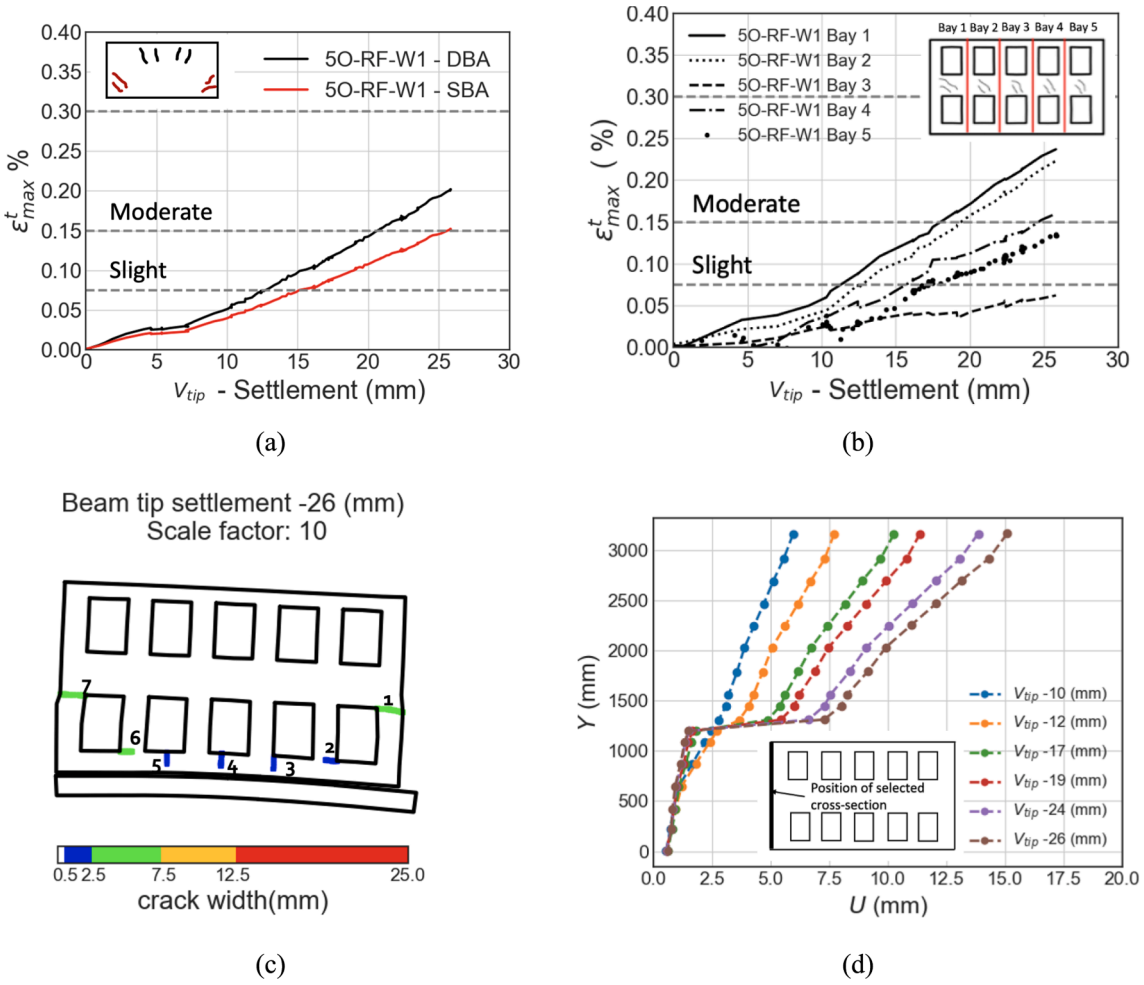

Fig. 6. (a) Values of maximum tensile strain ε^t_{max} estimated from measured values of deflection ratio and average horizontal strain for 50O-RF-W1 using the DBA (Black) and SBA (Red). Inset, illustration of the crack locations implied by the tensile strains estimated by the DBA (Black) and SBA (red). Horizontal dashed lines indicate boundaries of damage categories. The inset shows the potential damage locations; (b) Values of maximum tensile strain ε^t_{max} determined from angular distortion and average horizontal strain using the BBA for 50O-RF-W1. The division of bays is shown in the inset; (c) Deformed shape of the front façade of 50O-RF-W1 at a beam tip settlement of 26 mm, plotted with the crack location and size (indicated by the colour bar where blue and green, signify 'slight' and 'moderate' damage respectively). The deformed shape is displayed with an orientation that mirrors the perspective of facade-facing cameras; (d) Profiles of the cross-section at the left edge of the building model subjected various beam tip settlements for 50O-RF-W1. (For interpretation of the references to colour in this figure legend, the reader is referred to the web version of this article.)

Table 4
Summary of the performance of DBA, SBA and BBA equivalent beam models in terms of indicating damage category and location at the final stage of each test.

Test ID	Types	Observation[1]	DBA	SBA	BBA[2]
3O-RF-W1	Damage Category	Slight	Negligible	Negligible	Negligible
	Damage Location	–	Poor	Poor	Poor
3O-RF-W3	Damage Category	Severe	Moderate	Moderate	Severe
	Damage Location	–	Poor	Poor	Poor
3O-JF-W1	Damage Category	Very severe	Moderate	–	Slight
	Damage Location	–	Good	–	Poor
50O-RF-W1	Damage Category	Moderate	Moderate	Moderate	Moderate
	Damage Location	–	Poor	Poor	Poor

[1] Based on the maximum measured crack width (equivalent crack width for half-scale tests) and correlations presented in Table A1.
[2] Only the most severe damage category recorded.

relationship from the slight damage category (as indicated by blue colour in Fig. 7) up to the upper bound of the moderate damage category (as indicated by green colour in Fig. 7). However, when the standard correlations are applied there is a tendency for the estimated strain to imply a smaller maximum crack width than is actually observed. However, it should be noted that the approximately linear relationship in Fig. 7a-b no longer holds when very severe cracks occur (as was the case for cracks 1,2 and 3 in 3O-JF-W1 as shown in Fig. 5c); data on cracks 1,2 and 3 in 3O-JF-W1 are excluded from Fig. 7a. Conversely, when damage is local and small, notably in test 3O-RF-W1 in Fig. 7a-b, the tensile strain – crack width correlation departs from that of other tests, leading to further disagreement with the standard correlations.

Compared to DBA and SBA, the relationship between the calculated tensile strain using BBA and damage (Fig. 7c-d) in a specific bay, is more scattered. One of the reasons for the scatter relates to the arbitrary definition of building bays; it is difficult to define an appropriate mechanical model for bays. Moreover, BBA neglects bending deformations, which can be significant. For instance, when predicting the damage category of 3O-JF-W1, the behaviour of which strongly resembled a beam, the BBA approach was unable to capture the very severe damage level which is associated with a bending-type failure mode.

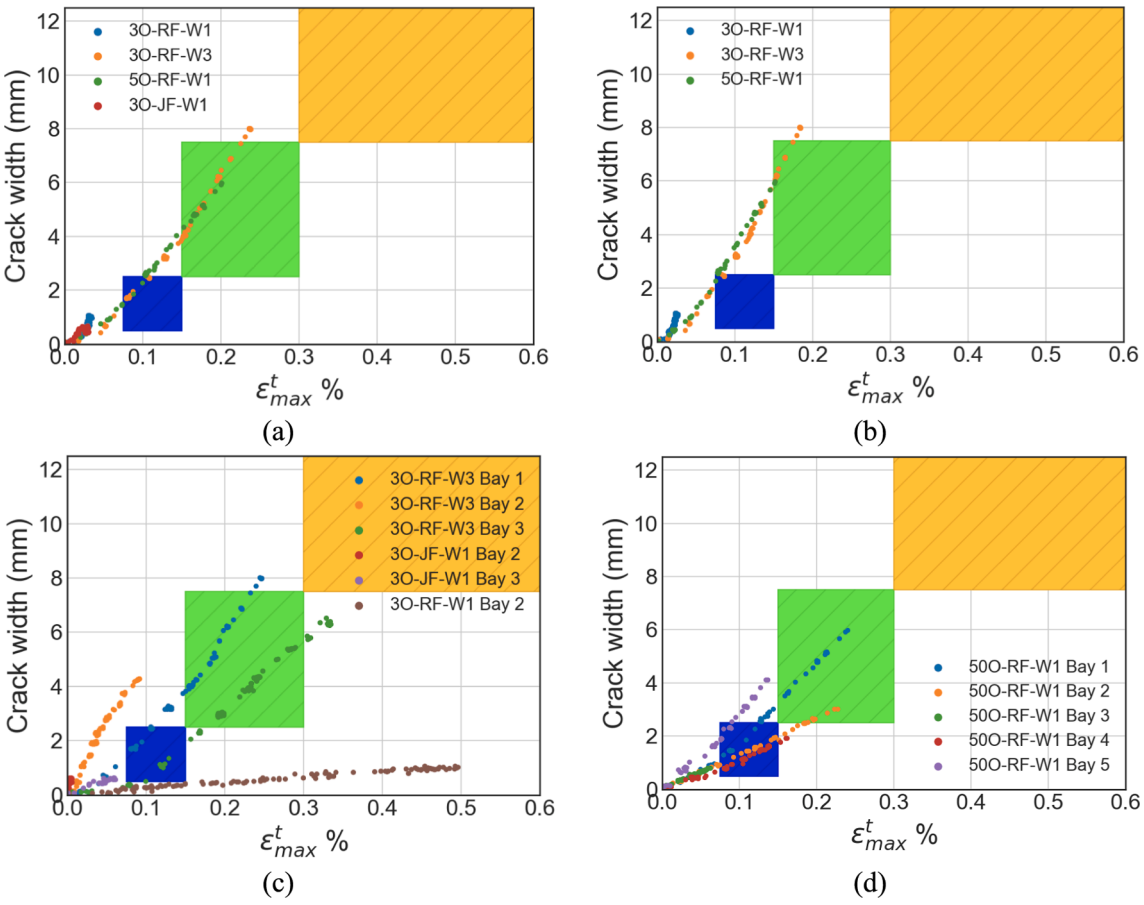

Fig. 7. Combined data for estimated maximum tensile strain plotted against maximum observed crack width for: (a) DBA; (b) SBA; (c) BBA (3 opening models); (d) BBA (5 opening models). Data on cracks 1, 2, and 3 in 3O-JF-W1 are excluded from Fig. 7a as they are beyond the regions of this figure. The hatched boxes indicate the standard correlations: blue, green, and amber colours correspond to the 'slight', 'moderate', and 'severe' damage categories, respectively (see Appendix A). (For interpretation of the references to colour in this figure legend, the reader is referred to the web version of this article.)

5. Equivalent frame idealisation (EFI)

Methods which idealise buildings as equivalent beams (i.e. DBA, SBA and BBA) have limited success in categorising and locating damage. Poor performance is largely due to a mismatch between the kinematics assumed in the beam models and the deformations experienced by the building. An alternative approach is therefore proposed, called the Equivalent Frame Idealisation (EFI), in which the building façade is

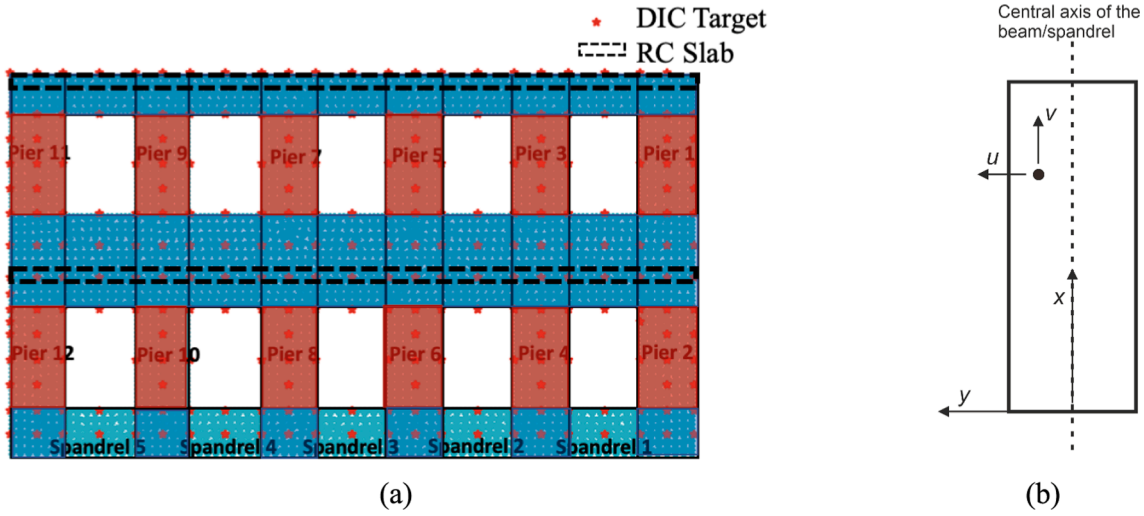

Fig. 8. (a) Discretisation of the 50O building model using Timoshenko beam elements and connectors. Red and green colours indicate structural components modelled as beams; connectors are indicated in blue. Red dots are DIC target locations at which displacement data are measured; The locations of reinforced concrete slabs are indicated by black boxes with dashed boundary lines. (b) A beam element showing the local coordinates (x, y) and corresponding displacements (u, v). (For interpretation of the references to colour in this figure legend, the reader is referred to the web version of this article.)

idealised as an equivalent frame. This approach can be viewed as a higher resolution version of the DBA; in DBA the whole façade is represented as a beam whereas in EFI the beam approximation is employed at the level of individual piers and spandrels.

In the EFI approach, building façades are considered to comprise three types of structural component: piers, spandrels and connectors. Fig. 8a for the 50O building model shows piers (coloured in red) and spandrels (at the bottom of the façade, coloured in green). 'Connectors' (coloured in blue in Fig. 8a) are typically employed to connect the piers and spandrels. Assumed displacement fields in the piers and spandrels, based on Timoshenko beam theory, facilitate the estimation of damage category in each component based on the magnitude of the inferred tensile strains. In contrast, the 'connectors' are treated as relatively rigid elements in which damage is unlikely; no attempt is made to estimate strain distributions in the connectors. In the building models with slab floors the spandrels in contact with the slabs did not experience any damage; this is presumably a consequence of the local reinforcing effect of the slab. For this reason, in the current work spandrels connected to slabs were treated as connectors (e.g. as shown in Fig. 8a for the spandrels at first and second floor levels).

5.1. Strain estimation

In contrast to the equivalent beam models, EFI does not require the definition of distortion measures to estimate strain. Displacement field functions from beam theory are directly fitted to the measured displacement data in a least squares sense. Partial derivatives of the displacement fields are then used to obtain the strain fields and estimate the maximum tensile strain in the element.

Consistent with Timoshenko beam theory the settlement-induced displacement field in each beam component is represented by,

$$u(x,y) = -\phi y + fx + e \tag{7}$$

$$v(x,y) = c_1x^3 + c_2x^2 + c_3x + c_4 \tag{8}$$

where x, y are local coordinates (Fig. 8b), u, v are corresponding displacements and f, e, c_1, c_2, c_3 and c_4 are kinematic parameters. Consistent with beam theory, plane sections remain plane; ϕ is the rotation of the beam cross section. The transverse settlement-induced shear strain is:

$$\gamma_{xy} = \frac{1}{2}\left(\frac{\partial u}{\partial y} + \frac{\partial v}{\partial x}\right) = \frac{1}{2}\left(\phi + \frac{\partial v}{\partial x}\right) \tag{9}$$

To emphasise that this expression for shear strain represents an averaged value over the cross section in the current model, the nomenclature $\gamma_{ave} = \gamma_{xy}$ is employed below.

It is considered that a set of displacement data (u_i, v_i) are available at locations (x_i, y_i) in the beam, where $i \in (1, 2, \cdots, n)$ is the index of the measurement target. The measured displacement data are related to the model parameters by,

$$\begin{bmatrix} u_1 \\ v_1 \\ u_2 \\ v_2 \\ \vdots \\ u_n \\ v_n \end{bmatrix} = \begin{bmatrix} -3y_1{x_1}^2 & -2y_1x_1 & -y_1 & 0 & x_1 & 1 & y_1 \\ {x_1}^3 & {x_1}^2 & x_1 & 1 & 0 & 0 & 0 \\ -3y_2{x_2}^2 & -2y_2x_2 & -y_2 & 0 & x_2 & 1 & y_2 \\ {x_2}^3 & {x_2}^2 & x_2 & 1 & 0 & 0 & 0 \\ \vdots & \vdots & \vdots & \vdots & \vdots & \vdots & \vdots \\ -3y_n{x_n}^2 & -2y_nx_n & -y_n & 0 & x_n & 1 & y_n \\ {x_n}^3 & {x_n}^2 & x_n & 1 & 0 & 0 & 0 \end{bmatrix} \begin{bmatrix} c_1 \\ c_2 \\ c_3 \\ c_4 \\ f \\ e \\ \gamma_{ave} \end{bmatrix} \tag{10}$$

Each measurement point provides horizontal u and vertical v displacement data, together with their corresponding coordinates (x, y). Since each measurement point provides two independent data (one for u and one for v), a minimum of four measurement points ($n = 4$) is required to obtain sufficient information to solve for seven unknown parameters in the model. With four measurement points, Equation 10 already becomes an overdetermined system. To minimise the influence of measurement errors, more than four measurement points should ideally be used for parameter evaluation, allowing for a more robust least squares solution. Once the parameters have been determined, the derived average shear strain γ_{ave} is re-distributed along the cross-section using a parabolic function satisfying zero shear strain conditions on the outer fibres of the cross-section. The axial strains within each beam element are then determined straightforwardly from Equations (7) and (8) and combined with re-distributed shear strains using a tensor-based approach to determine the maximum tensile strain ε^t_{max} in each pier and spandrel.

5.2. Application of the EFI to the experimental data

5.2.1. Example strain analysis for 3O-RF-W3

Fig. 9 illustrates the estimated strain distribution determined for the right external pier (indicated by the hatched area in Fig. 4d inset) of 3O-RF-W3 at various beam tip settlements. The arrows in Fig. 9 indicate the direction of the maximum principal strains, with their lengths proportional to the magnitudes of the strains. At 8 mm settlement, the EFI results in Fig. 9a show tensile strain concentrations at the upper left and lower right corners. At this stage in the test, no damage was observed in the pier, and the strain distribution derived from EFI conformed to expected deformation patterns. The root-mean-square error (RMSE) of 6.25×10^{-2} mm between measured and fitted displacements over 9 DIC targets suggests the kinematics of the pier is reasonably captured by EFI. As the settlement increased to 10 mm, the maximum tensile strain rose to 838 $\mu\varepsilon$. A crack emerged at the lower right corner of the pier (where tensile strains are concentrated) at 9.6 mm settlement. Its width was measured as 0.58 mm at 10 mm settlement. The RMSE was 8.16×10^{-2} mm at this stage. When the settlement reached 12 mm, the maximum tensile strain increased to 902 $\mu\varepsilon$, with a maximum crack width of 0.88 mm. The RMSE remained relatively small at 1.09×10^{-1} mm, suggesting that, despite the development of the crack (and the likely departure of the local kinematics from beam theory), strain distributions estimated from EFI provide a reasonable representation of the deformation. When the settlement increased to 16 mm, the maximum tensile strain reached 2327 $\mu\varepsilon$, and the crack widened to 1.67 mm. This relatively large crack significantly impacts the interpreted strain results (Fig. 9d), which appear to indicate large axial tensile strains across the height of the beam, as seen in the directions of the maximum principal strains (Fig. 9d), instead of reflecting the observed horizontal cracks at the top and bottom edges of the pier (Fig. 4c). Correspondingly, the RMSE increases to 4.17×10^{-1} mm. Despite this increase, it is observed that during the crack development, the maximum tensile strain grows commensurately with crack width. However, it is noteworthy that the observed crack width-maximum tensile strain relationship differs considerably from the standard correlation in Appendix A.

5.2.2. Tensile strain – Damage correlation

To further explore and generalise the observations in Sections 5.2.1, the maximum tensile strain ε^t_{max} in each pier and spandrel is determined from the DIC measurements employing the procedures in Section 5.1 at each stage in each of the building tests. The maximum crack width observed in each individual pier and spandrel is then compared with the maximum tensile strain estimated from the EFI in the same pier/spandrel that experienced the crack. The resulting data – collected together from all of the four building tests – are illustrated in Fig. 10a, with the hatched boxes indicating the standard correlations.

The data in Fig. 10a indicate a remarkably consistent linear correlation between maximum tensile strain and maximum observed crack width. However, the correlation does not map well onto the standard tensile strain – crack width correlations; data from the EFI suggest that

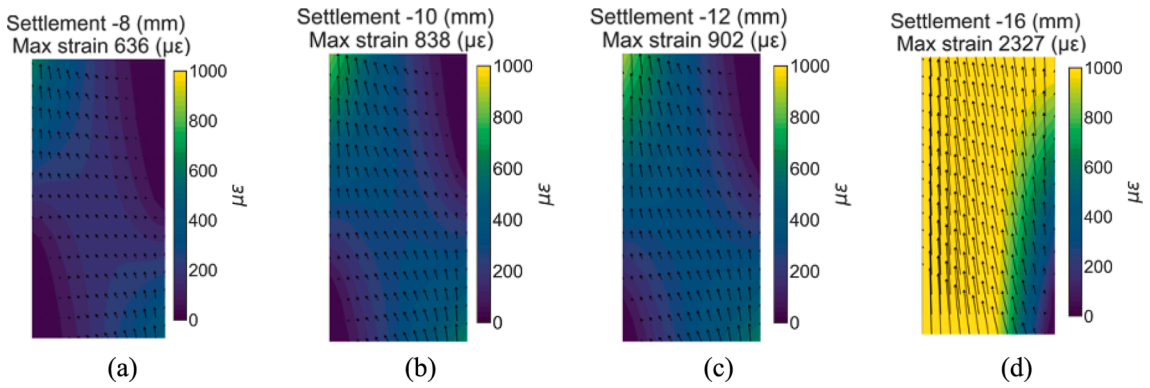

Fig. 9. Interpreted tensile principal strain distribution using EFI for the right external pier of 3O-RF-W3 at a beam tip settlement of (a) 8 mm; (b) 10 mm; (c) 12 mm; (d) 16 mm. The arrows in each figure indicate the direction of maximum principal strains, with their lengths proportional to the magnitudes of the strains. Note that in (d) the maximum strain (2327 με) lies above the adopted contour scale.

maximum observed crack widths correlate with larger strain magnitudes than is the case with the standard correlations. This inconsistency is unsurprising; the EFI is able to resolve localised concentrations of strain that are effectively 'smeared out' by the more coarsely-resolved equivalent beam methods.

An alternative strain-damage correlation is therefore proposed as indicated in Table 5; these correlations are illustrated in Fig. 10b. It is clear that the alternative correlations provide an improved representation of the data.

5.2.3. Crack size – Tensile strain maps

Maps have been developed in which individual piers and spandrels (elements highlighted with a black boundary in Figs. 11 and 12) are colour coded according to their damage category. The damage category is determined in two ways. Approach 1 uses the maximum observed crack width in the pier/spandrel to derive the damage category (following the standard damage category – crack width correlation in Table A1, at half-scale). Approach 2 uses the maximum tensile strain estimated from EFI to determine the damage category on the basis of the correlation in Table 5.

Maps for 3O-RF-W3 are indicated in Fig. 11, using Approach 1 (left column) and Approach 2 (right column), for increasing beam tip settlement. These maps demonstrate good agreement between damage category assigned from crack width measurements (Approach 1) and from the proposed crack size – strain correlation (Approach 2). There

Table 5
Proposed damage classification for use with the EFI approach.

Damage category	Crack width (at prototype scale)	Crack width (at model scale)	Strain range
Slight	1.0 – 5.0	0.5 – 2.5	0.125 % – 0.625 %
Moderate	5.0 – 15.0	2.5 – 7.5	0.625 % – 1.875 %
Severe	15.0 – 25.0	7.5 – 12.5	1.875 % – 3.125 %

are, however, some discrepancies. From an early stage in the test the right external pier on the first storey has been assigned a slight damage category in Approach 2, despite no crack being observed in this pier. There is also a slight mismatch between implied damage categories for the right internal pier on the ground storey during the later stages of settlement. On the basis of observed crack width, the damage would be classified as 'moderate' whereas – on the basis of the EFI– the damage is classified as 'slight'. In fact, the EFI estimate for the maximum tensile strain in this pier is only marginally less than the slight-moderate threshold.

It is clear that the EFI combined with the proposed tensile strain damage criteria is highly effective at identifying the presence of cracks. While some 'very slight' cracks (smaller than 0.5 mm) are observed on

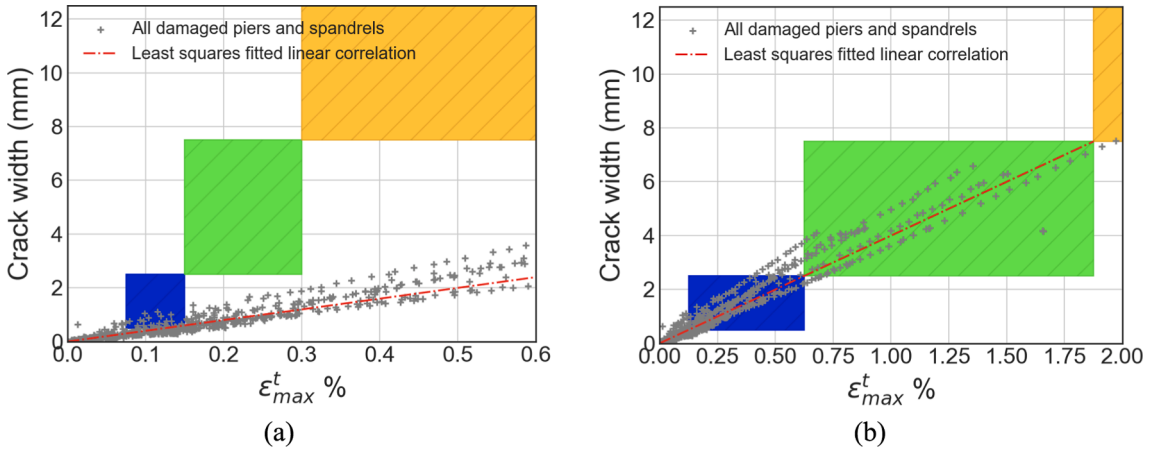

Fig. 10. (a) Correlation between maximum tensile strain (ε^t_{max}) estimated from the EFI and observed maximum crack width for all damaged piers and spandrels of all four building tests (14 no. in total), except for two piers from 3O-JF-W1 that developed anomalously large cracks, which are beyond the crack width range displayed in this figure. The hatched boxes indicate the standard correlations: blue, green, and amber colours correspond to the 'slight', 'moderate', and 'severe' damage categories, respectively (see Appendix A); (b) Alternative plot with re-scaled ε^t_{max} axis showing proposed strain-crack width correlations for the EFI approach. (For interpretation of the references to colour in this figure legend, the reader is referred to the web version of this article.)

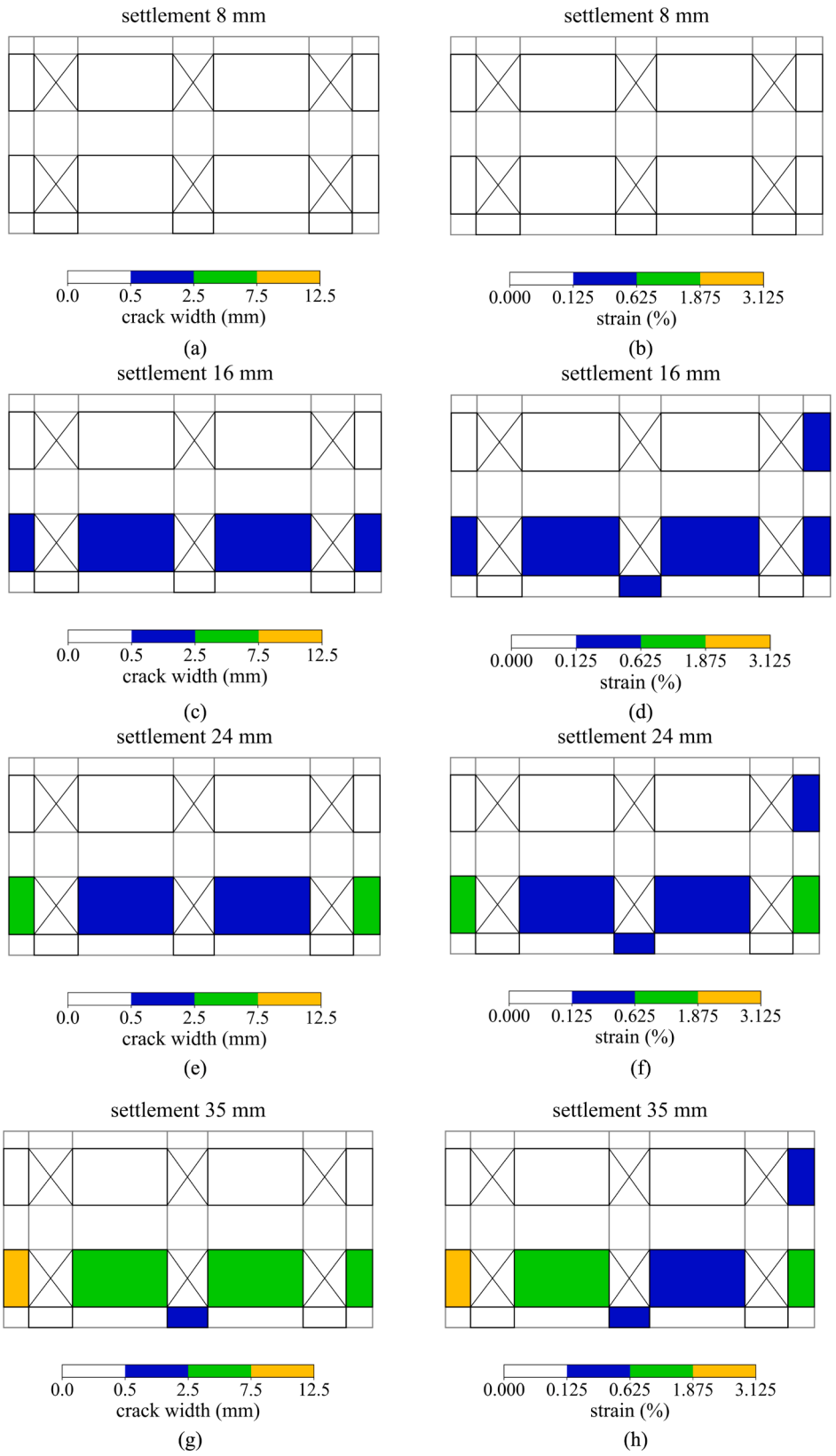

Fig. 11. (a)(c)(e)(g) Damage category of pier and spandrel components (highlighted with black boundary lines) of 3O-RF-W3 based on the maximum observed crack width at 8, 16 and 24 and 35 mm beam tip settlements (Approach 1); (b) (d)(f)(h) Damage category of pier and spandrel components (highlighted with black boundary lines) of 3O-RF-W3 based on the maximum interpreted tensile strain from the EFI at 8, 16, 24 and 35 mm beam tip settlements (Approach 2). Two additional targets above the left external pier on the ground storey were used in EFA to derive maximum tensile strain, due the observed crack (crack 1 in Fig. 4c) running through DIC targets placed at the top of the pier. The diagonal crosses in the maps denote window opening.

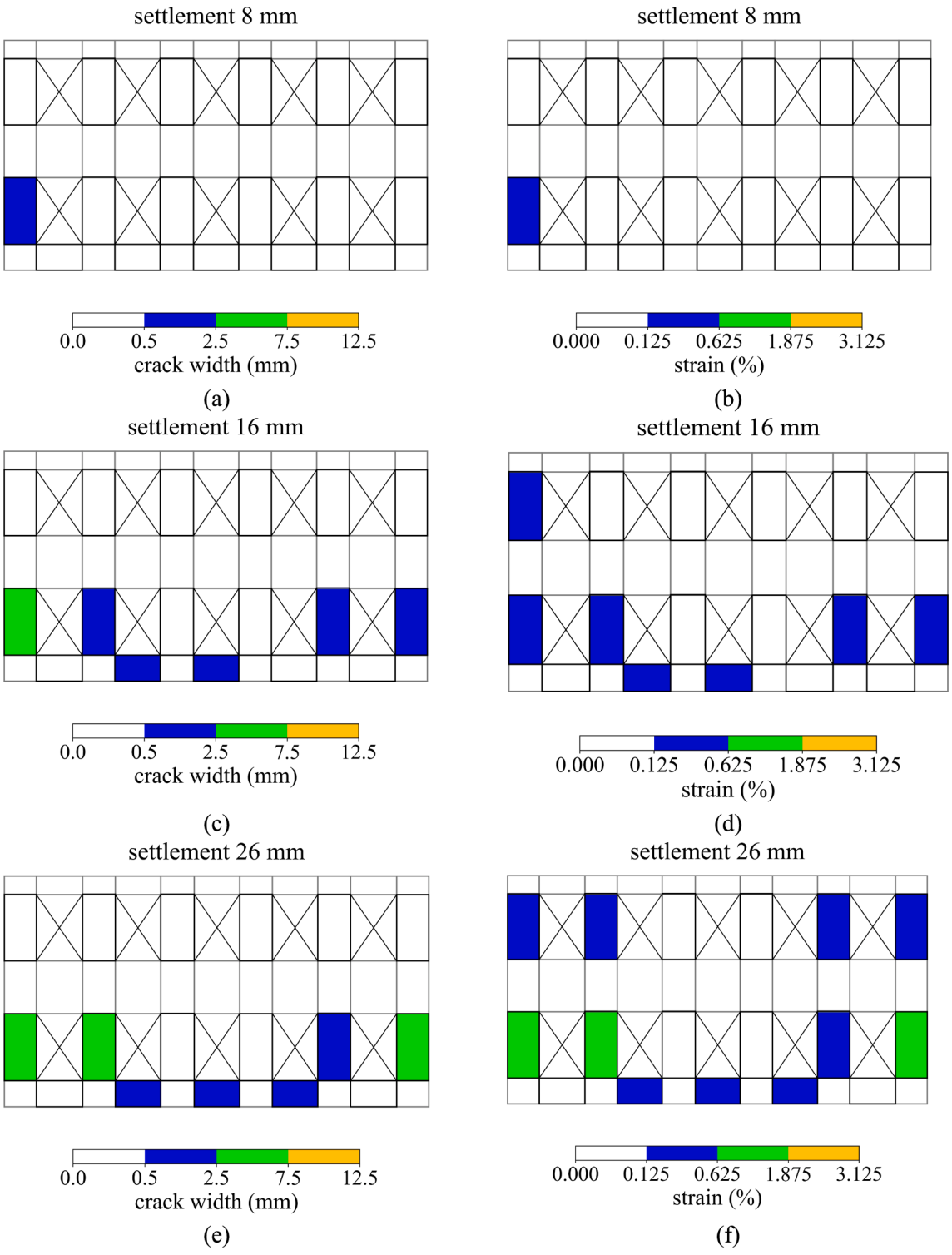

Fig. 12. (a)(c)(e) Damage category in pier and spandrel components (highlighted with black boundary lines) for 50O-RF-W1 based on the maximum observed crack width at 8, 16 and 26 mm beam tip settlements; (b)(d)(f) Damage category of pier and spandrel components (highlighted with black boundary lines) for 50O-RF-W1 based on the maximum estimated tensile strain from the EFI using DIC displacement data at targets at 8, 16, 26 mm beam tip settlements. Three additional targets above the right external pier on the ground storey were used in EFI to derive maximum tensile strain, due the observed crack (crack 1 in Fig. 6c) running through DIC targets placed at the top of the pier.

the piers of the first storey, suggesting that the damage category may be overestimated based on the estimated tensile strain, it is also possible that other small cracks, which could qualify the pier for the slight damage category, were missed at this less accessible location. An increase in maximum tensile strains on the first storey is likely a result of the observed considerable bending in external piers. This suggestion is supported by the distortions evident in Fig. 6d and earlier numerical simulations by Dalgic et al. (2021).

In all examined cases, the EFI located and captured the propagation of the damage reasonably well. The method highlights, from early

stages, structural components which are experiencing distress, enabling further monitoring and intervention activities.

6. Discussion

The use of equivalent beam models (DBA, SBA and BBA) and standard damage-crack width-tensile strain relationships to estimate damage from displacement measurements provides low fidelity results. The damage category cannot be determined using these models in a consistently reliable way and the observed cracking damage tends to occur at locations that are inconsistent with the underlying beam theory assumptions. It is noted that this empirical damage assessment procedure has been developed over many years; numerical values of the widely-accepted crack width-tensile strain correlations that are embedded in this approach appear to be tailored to provide an approximate match between observed damage on the one hand and estimated tensile strain on the other. Within this context, the standard damage category-crack width-tensile strain correlations should not be regarded as having a fundamental basis; instead, they represent a numerical correlation that – when employed with equivalent beam models – appear to provide an indication of observed building damage. This suggests that the standard numerical damage – tensile strain correlations have effectively been 'tuned' to compensate for deficiencies in the beam modelling approach when applied to real buildings. The application of the equivalent beam-based damage assessment approach to building models demonstrates that the method is capable of indicating the presence of damage, but damage categories are often underestimated. While alternative strain – damage correlations could be proposed to improve the performance of this approach, the fundamental limitation of equivalent beam models in failing to capture the building kinematics and locating damage cannot be resolved.

The EFI approach presented in this paper is a higher fidelity procedure in which beam models are applied to the individual piers and spandrels in the building. The EFI approach is shown to provide an excellent indication of damage, in terms of both intensity and location. A key finding, however, is that the standard crack width-tensile strain correlation does not appear to be appropriate for the EFI approach. An alternative correlation – in which the limiting tensile strain values are larger than those in the standard correlation, see Table 5 – is proposed for use with EFI. To highlight the need for a new correlation an exercise has been conducted in which – for each building at each stage in the test – values of maximum tensile strain estimated from the DBA are compared with maximum tensile strain (for the façade as a whole) estimated from the EFI. Results are plotted in Fig. 13. It is clear that the strains detected by the EFI are systematically larger than those estimated by the DBA. This is an unsurprising outcome; the presence of openings in the façade would be expected to concentrate building strains in the piers and spandrels. It is not claimed that the data in Table 5 represent a definitive correlation for future damage assessment analysis; in particular the cracks sizes relate to a half-size building and it is considered that scaling would need to be applied for applications to full-size buildings. Further work is needed to confirm the numerical values of the correlations and also to consider whether they should incorporate a representation of masonry material parameters. It is concluded, however, that the appropriate correlations between tensile strain and crack damage – when tensile strains are calculated at the level of individual piers/spandrels – will be expected to differ considerably from the standard correlations.

The adoption of higher fidelity methods for damage assessment, such as the EFI, require a larger number of displacement measurement points than typically adopted in current practice. While DIC was used to obtain the experimental data in this paper, site surveying techniques commonly used for displacement monitoring, such as electronic distance measurement using total stations, could also be employed. The authors have developed laser scan displacement monitoring techniques (see initial work in this area Liu et al., 2022a) which may also provide an attractive

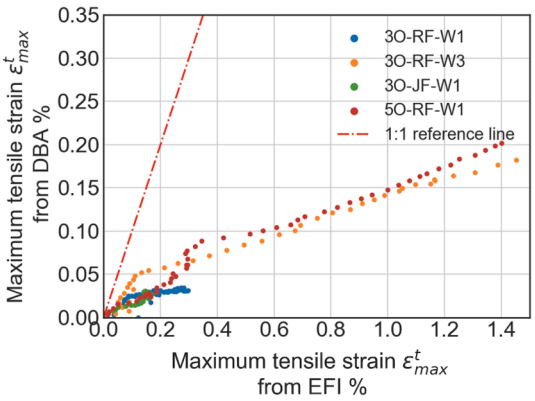

Fig. 13. Maximum values of estimated tensile strain from the DBA compared with maximum values of estimated tensile strain of all piers and spandrel components of the same building model from the EFI throughout each test. The 1:1 reference line denotes the hypothetical scenario where estimated tensile strains from DBA are equal to those from EFI.

option. It is noted that with EFI it is not necessary to choose specific locations to measure building displacements. The method is tolerant of incomplete displacement data (provided that a suitable minimum of data are available); it is therefore robust against occlusions. The results obtained in this paper indicate that the method is able to handle noise on the DIC data.

It is important to emphasise that this paper is not on the numerical modelling of masonry buildings. Instead, it conducts a performance assessment of equivalent beam approaches using full field monitoring data, before proposing an alternative representation based on the concept of an equivalent frame. The remarkably consistent linear correlation between maximum tensile strain and maximum observed crack width (as plotted in Fig. 10) across all structural components and all building models supports the approach's general applicability. During the development of the methods described in this paper, the validity of EFI as a monitoring approach was evaluated numerically using 3D nonlinear finite element models of the test buildings; details are provided in Liu (2023).

Although the current paper is concerned with the processing of monitored data, the findings have implications for the prediction of damage categories within a building prior to underground construction. In current practice, the damage category is typically predicted by applying assumed ground movements to an equivalent beam model of the building and classifying the damage on the basis of the standard correlations. If alternative assessment procedures are used in which a higher fidelity structural analysis (such as an equivalent frame model, Gulen et al. (2024), or a finite element model) is used, then the adoption of the standard tensile crack width – tensile strain correlation could lead to over-conservative damage assessments.

7. Summary

This paper investigated the performance of techniques which estimate settlement-induced damage in masonry buildings using displacement measurements and various equivalent beam idealisations (Timoshenko, sandwich and bay beams). To do this, detailed displacement data collected during a large-scale settlement test campaign on model masonry buildings with different openings and floor structures were used. By comparing the predicted damage category obtained via equivalent beam models with the damage category results based on detailed crack monitoring, it was observed that the accuracy of building damage categories estimated from beam idealisation relies on the assumed relationship between the estimated maximum strains and damage category. Using standard correlations with equivalent beam models often led to an underestimation of damage category. More

importantly, the results demonstrated that crack locations and patterns implied by beam models could be significantly different from the observed damage due to a mismatch between beam and building kinematics.

As an alternative, a strain interpretation routine called EFI that idealises the façade as an equivalent frame was proposed. In this approach, individual piers and spandrels, instead of the whole façade, were modelled by using displacement fields based on Timoshenko beam idealisations to achieve higher resolution and fidelity. The experimental data revealed a linear relationship between maximum crack width and EFI estimated maximum strain for individual piers and spandrels. It was also shown that the standard crack width-tensile strain correlation did not appear to be appropriate on individual structural components' level, highlighting the need for a re-calibration of these correlations for high-resolution structural idealisations. After a re-calibration of the standard correlations, the EFI approach was shown to provide an excellent indication of damage, both in terms of location and intensity, for all the examined building configurations. The proposed EFI approach therefore appears to offer improved performance than current methods based on equivalent beams.

CRediT authorship contribution statement

Yiyan Liu: Writing – original draft, Visualization, Validation, Software, Investigation, Formal analysis, Data curation, Conceptualization. **Harvey Burd:** Writing – review & editing, Supervision, Methodology, Conceptualization. **Derya Burcu Gulen:** Software, Investigation, Data curation. **Korhan Deniz Dalgic:** Writing – review & editing, Resources, Investigation. **Ben Gilson:** Writing – review & editing, Supervision. **Alper Ilki:** Writing – review & editing, Investigation. **Sinan Acikgoz:** Writing – review & editing, Supervision, Resources, Project administration, Methodology, Funding acquisition, Conceptualization.

Declaration of competing interest

The authors declare that they have no known competing financial interests or personal relationships that could have appeared to influence the work reported in this paper.

Acknowledgements

The authors wish to acknowledge the contributions of the Fibrobeton staff, especially Mr. Muhammed Maraşlı and Mr. Hasan Bilgin. The first author would also like to thank Arup for funding his research through an EPSRC iCASE. Additionally, the second and seventh authors wish to express their gratitude to the Institution of Structural Engineers (IStructE) for supporting the experimental work presented in this paper with the 2020 IStructE Research Award.

Appendix A. – Standard damage correlations

.

Table A1
Damage correlations based on data from Burland et al. (1977) and Boscardin and Cording (1989).

Damage category	Severity	Crack width	Equivalent crack width for half-scale tests	Limiting tensile strain
0	Negligible	Less than 0.1 mm	Less than 0.05 mm	0–0.05
1	Very slight	Up to 1 mm	Up to 0.5 mm	0.05–0.075
2	Slight	Up to 5 mm	Up to 2.5 mm	0.075–0.15
3	Moderate	Between 5 mm and 15 mm or several greater then 3 mm	Between 2.5 mm and 7.5 mm or several greater then 1.5 mm	0.15–0.3
4	Severe	15 mm to 25 mm	7.5 mm to 12.5 mm	Greater than 0.3
5	Very severe	Greater than 25 mm	Greater than 12.5 mm	

Data availability

Data will be made available on request.

References

Boscardin, M.D., Cording, E.J., 1989. Building response to excavation-induced settlement. J. Geotech. Eng. 115, 1–21.
Burland, J.B., Broms, B.B., De Mello, V.F.B., 1977. Behavior of foundations and structures. In: Proc., 9th Int. Conf. on Soil Mechanics and Foundation Engineering, pp. 495–546.
Burland, J.B., Wroth, C.P., 1974. Settlement of buildings and associated damage. In: In: Settlement of Structures, Proceedings of the Conference of the British Geotechnical Society, pp. 611–654.
Cook, D., 1994. Studies of Settlement and Crack Damage in Old and New Facades. In: Proceedings of 3rd International Masonry Conference. British Masonry Society, pp. 203–211.
Dalgic, K.D., Gulen, D.B., Acikgoz, S., Burd, H., Hendriks, M.A.N., Giardina, G., Ilki, A., 2021. Large Scale Experimental Settlement Tests to Evaluate Structural Models for Tunnelling-Induced Damage Analysis. In: Barla, M., Di Donna, A., Sterpi, D. (Eds.), Challenges and Innovations in Geomechanics. Springer International Publishing, Cham, pp. 164–171.
Dalgic, K.D., Gulen, B., Liu, Y., Acikgoz, S., Burd, H., Marasli, M., Ilki, A., 2023. Masonry buildings subjected to settlements: Half-scale testing, detailed measurements, and insights into behaviour. Eng Struct 278, 115233.
Finno, R.J., Voss, F.T., Rossow, E., Blackburn, J.T., 2005. Evaluating Damage Potential in Buildings Affected by Excavations. J. Geotech. Geoenviron. Eng. 131, 1199–1210.
Giardina, G., van de Graaf, A.V., Hendriks, M.A.N., Rots, J.G., Marini, A., 2013. Numerical analysis of a masonry façade subject to tunnelling-induced settlements. Eng Struct 54, 234–247.
Gulen, D.B., Acikgoz, S., Burd, H., 2021. Equivalent frame model for the assessment of tunnel-induced damage to masonry buildings. In: Elshafie, M.Z.E.B., Viggiani, G.M. B., Mair, R.J. (Eds.), Geotechnical Aspects of Underground Construction in Soft Ground. CRC Press.
Gulen, D.B., Acikgoz, S., Burd, H.J., 2024. Equivalent Frame Model with Deformable Connectors to Assess Tunnelling-Induced Damage to Masonry Buildings, SSRN. https://ssrn.com/abstract=4977873.
High Speed Two Limited, 2017. High Speed Two Phase One C3 : Ground Settlement [WWW Document]. URL https://assets.publishing.service.gov.uk/government/uploads/system/uploads/attachment_data/file/672194/C3_-_Ground_Settlement_v1.pdf (accessed 7.28.20).
ITA/AITES, 2011. Monitoring and control in tunnel construction, ITA Report 9.
Lagomarsino, S., Penna, A., Galasco, A., Cattari, S., 2013. TREMURI program: An equivalent frame model for the nonlinear seismic analysis of masonry buildings. Eng Struct 56, 1787–1799.
Crossrail Limited, 2008. Crossrail Information Paper D12 – Ground Settlement [WWW Document]. URL http://74f85f59f39b887b696f-ab656259048fb93837ecc0ecbcf0c557.r23.cf3.rackcdn.com/assets/library/document/d/original/d12groundsettlement.pdf (accessed 7.28.20).
Liu, Y., 2023. Displacement and Damage Monitoring for Masonry Buildings Subjected to Ground Movements Induced by Underground Construction (DPhil Thesis). University of Oxford, Oxford.

Liu, Y., Acikgoz, S., Burd, H., 2022a. Terrestrial Laser Scanning based deformation monitoring for masonry buildings subjected to settlement induced by underground construction. In: García-Asenjo, L., Lerma, J.L. (Eds.), Proceedings of the 5th Joint International Symposium on Deformation Monitoring - JISDM 2022. Editorial Universitat Politècnica de València, Valencia, pp. 375–382.

Liu, Y., Gulen, B., Acikgoz, S., Burd, H., Gilson, B., Ilki, A., Dalgic, K.D., 2022b. A critical evaluation of proxy measures used to quantify excavation-induced damage in masonry buildings. In: Lancellotta, R., Viggiani, C., Flora, A., de Silva, F., Mele, L. (Eds.), Geotechnical Engineering for the Preservation of Monuments and Historic Sites III. CRC Press, pp. 1015–1025.

Mair, R.J., 1998. Recent experiences of tunneling and deep excavations in London SOA-7. In: In: 1998-Fourth International Conference on Case Histories in Geotechnical Engineering, pp. 1193–1206.

Mair, R.J., Taylor, R.N., Burland, J.B., 1996. Prediction of ground movements and assessment of risk of building damage due to bored tunnelling. Geotechnical Aspects of Underground Construction in Soft Ground 713–718.

Ritter, S., Giardina, G., Franza, A., DeJong, M.J., 2020. Building Deformation Caused by Tunneling: Centrifuge Modeling. J. Geotech. Geoenviron. Eng. 146, 04020017.

Skempton, A.W., MacDonald, D.H., 1956. The allowable settlements of buildings. In: In: Proceedings of the Institution of Civil Engineers, pp. 727–768.

Son, M., Cording, E.J., 2005. Estimation of Building Damage Due to Excavation-Induced Ground Movements. J. Geotech. Geoenviron. Eng. 131, 162–177.

Thames Water Utilities Limited, 2014. Thames Tideway Tunnel Settlement Information Paper [WWW Document]. URL https://www.tideway.london/media/3075/app191-settlement-information-paper-3-march-2014.pdf (accessed 7.28.20).